Applied Catalysis B: Environmental 156–157 (2014) 301–306

Contents lists available at ScienceDirect

Applied Catalysis B: Environmental

journal homepage: www.elsevier.com/locate/apcatb

The role of water in the degradation of Pt_3Co/C nanoparticles: An Identical Location Transmission Electron Microscopy study in polymer electrolyte environment

Flávio R. Nikkuni[a,b,c,2], Benoit Vion-Dury[a,b], Laetitia Dubau[a,b], Frédéric Maillard[a,b], Edson A. Ticianelli[c], Marian Chatenet[a,b,*,1]

[a] Univ. Grenoble Alpes, LEPMI, F-38000 Grenoble, France
[b] CNRS, LEPMI, F-38000 Grenoble, France
[c] Instituto de Química de São Carlos, U. de São Paulo, Avenida Trabalhador Sãocarlense, 400 Parque Arnold Schmidt, CP 780, 13560-970 São Carlos, SP, Brazil

ARTICLE INFO

Article history:
Received 2 December 2013
Received in revised form 11 March 2014
Accepted 13 March 2014
Available online 21 March 2014

Keywords:
Identical Location Transmission Electron Microscopy (IL-TEM)
Ultramicroelectrode with cavity (UMEC)
Oxygen reduction reaction (ORR)
Platinum–cobalt nanostructured electrocatalyst degradation
Nafion® polymer electrolyte

ABSTRACT

The degradation mechanisms of nanostructured Pt_3Co/C electrocatalysts aged in dry electrochemical environment using a Nafion® 115 membrane as polymer electrolyte were characterized by Identical Location Transmission Electron Microscopy, in conditions that perfectly mimic real PEMFC operation. The structural, morphological and compositional changes of the Pt_3Co/C nanoparticles occurring during an accelerated stress test were bridged to changes of their intrinsic kinetics toward the oxygen reduction reaction in Nafion® 115 electrolyte, thanks to an ultramicroelectrode with cavity loaded with the catalyst. The unique setup used herein further enabled to compare the Nafion® environment with conventional liquid electrolyte in which accelerated stress tests are usually performed. Although the Pt_3Co/C nanoparticles are modified upon aging at Nafion® interface, the degradation processes are milder and different than those observed in liquid electrolyte, mostly following the absence of liquid water and the lack of ion mobility within the Nafion® membrane.

1. Introduction

As most sustainable energy conversion and storage devices, proton exchange membrane fuel cells (PEMFCs) rely on electrocatalytic reactions [1,2]. Using platinum-based nanocrystallites deposited on high surface area carbon (Pt-M/C, with M = Co, Ni or Cu) in PEMFC cathodes enables to accelerate the sluggish oxygen reduction reaction (ORR) and to improve the catalytic layer durability [3–7]. These materials activity depends on their structure, morphology, composition and particle size [6–12], features that undergo severe modification upon PEMFC operation [13–18]. Thus, the research effort to elucidate their extent and mechanisms of degradation, *via* Accelerated Stress Tests (AST), is intense [19–26]. AST are usually performed in aqueous electrolyte solutions, which is not without consequence, because water participates to the degradation mechanisms of Pt-M/C electrocatalysts [27,28]. This puts into question the relevance of such AST to mimic real PEMFC degradations.

This paper explores the role played by the electrolyte, and thus the role of water, in the degradation mechanisms of state-of-the-art Pt-M/C electrocatalysts. To this fundamental and technologically-relevant goal, AST were performed in a "dry cell", using an ultramicroelectrode with cavity (UMEC) filled with Pt_3Co/C nanoparticles as the working electrode and a Nafion® 115 membrane as the electrolyte (Supplementary Fig. S1). Combining the dry cell with an UMEC enabled measuring the intrinsic ORR kinetics of the electrocatalyst at the interface with Nafion®, which perfectly mimics the operating conditions of a PEMFC [29,30]. In complement, the Pt_3Co/C electrocatalyst was immobilized onto a gold TEM grid to monitor the structural and chemical changes of identical alloy nanoparticles prior/after the AST using Identical Location Transmission Electron Microscopy (IL-TEM). For comparison purposes, the experiments were reproduced in liquid electrolyte (same electrocatalyst, potential variations and test durations) and in a single PEMFC. As demonstrated hereafter, the dry cell provides unique information, out of reach from conventional electrochemical techniques, to understand the role played by water in the degradation of Pt-M/C materials.

* Corresponding author. Tel.: +33 476 826 588; fax: +33 476 826 777.
E-mail address: Marian.Chatenet@grenoble-inp.fr (M. Chatenet).
[1] Member of the French University Institute (IUF).
[2] Present address: Fundação Parque Tecnológico Itaipu – Projeto baterias, Av. Tancredo Neves, 6731, Caixa Postal 2039, CEP 85.867-900, Foz do Iguaçu, Paraná, Brazil.

http://dx.doi.org/10.1016/j.apcatb.2014.03.029
0926-3373/

2. Experimental

2.1. Materials and devices

The TEM micrographs were obtained on a JEOL 2010 TEM apparatus, equipped with a LaB_6 filament operating at 200 kV (point to point resolution 0.19 Å) and an X-ray energy dispersive spectrometer: X-EDS, Oxford – INCA®. The Pt_3Co/C powder was deposited onto a gold TEM grid with Lacey carbon membrane compatible with immersion in electrochemical medium. All the electrochemical experiments (characterization and accelerated stress test procedures) were conducted using a computer-controlled numerical potentiostat (Autolab PGSTAT302N).

The electrochemical aging and characterization experiments were performed in a dry cell employing a Nafion® 115 polymer electrolyte, a gold UMEC working electrode loaded with Pt_3Co/C (E-Tek, 20% weight fraction, Vulcan XC72 carbon black substrate), a Pt mesh counter electrode and a freshly-prepared reversible hydrogen electrode (reference). The dry cell, UMEC and IL-TEM techniques are detailed in Supplementary Fig. S1 and in Refs. [19,30–32]. The way the UMEC can be filled/emptied by/from the Pt_3Co/C catalytic powder is thoroughly detailed in reference [32]. The in-house designed and built dry cell consists of a Kel-F base onto which a Kel-F upside-down U-cup cover is attached. The base supports the polymer electrolyte membrane (Nafion® 115), which separates the ultramicroelectrode with cavity loaded with the catalyst powder (on the lower side of the membrane) from the Pt-mesh counter-electrode (facing the UMEC, on the upper side of the membrane). The reversible hydrogen electrode (RHE) used as reference electrode consists of a Pt wire immersed in 0.5 mol L^{-1} H_2SO_4 aqueous solution (and in contact with an electrogenerated hydrogen bubble), at the tip of which a very fine glass capillary is contacted with the Nafion® membrane to enable ionic percolation with the UMEC. The Nafion® membrane was immersed in sulfuric acid and then boiled in water, for cleaning and regeneration (into the protonated form) of its sulfonic groups prior each experiment. The tip of the RHE is located *ca.* 2 cm away from the UMEC and on the other side of the polymer membrane, to avoid contamination of the UMEC by aqueous H_2SO_4. During the whole experiment (aging or characterization procedure), the cell is fed with fully humidified gases (argon or oxygen, all in high purity, Air Liquide®) on both side of the membrane.

2.2. Electrochemical procedures

The accelerated stress test (AST) performed on the Pt_3Co/C electrocatalyst filling the UMEC or immobilized onto the gold TEM grid consists of alternating 60 s-long potential steps at $E = 0.1$ and 0.9 V *vs.* RHE during 15 h under argon atmosphere, at room temperature ($T = 298 \pm 2$ K). During the whole AST procedure and the ORR characterizations, the UMEC (or gold TEM grid) remained at the interface with a 115 Nafion® membrane in the absence of any liquid electrolyte. The electrochemical characterizations applied prior/after the AST consisted firstly of a base voltamperogram in the dry cell (Ar atmosphere), followed by a CO-stripping voltammogram in 1.0 mol L^{-1} H_2SO_4 aqueous solution (6 min under CO followed by 39 min flush under argon, the electrode potential being maintained at $E = 0.1$ V *vs.* RHE, followed by 3 CV cycles in the range $E = 0.05$–1.2 V *vs.* RHE at $v = 20$ mV s^{-1}) to measure the electroactive area of the Pt_3Co/C nanoparticles (procedure described in supplementary information; see also Supplementary Fig. S2). Then, the UMEC was thoroughly washed in water to remove any trace of H_2SO_4 and brought back to the dry cell, where quasi-stationary (1 mV s^{-1}) oxygen reduction voltamperometry was performed between $E = 1.05$ and 0.3 V *vs.* RHE to probe the intrinsic ORR activity of the electrocatalyst immobilized in the UMEC, this characterization being performed prior/after the AST in the dry cell. Overall, the procedures are similar to those performed in reference [19], except Nafion® polymer electrolyte is used instead of 1.0 mol L^{-1} sulfuric acid solution for the ORR and AST. In all intrinsic ORR activity determination, the limiting current taken into account in the calculation was always extracted from the experiment considered (*i.e.* prior and after aging), and the active area calculated from the CO-stripping voltamperograms.

Table 1
Mean Pt-Co/C particle diameter (d_{Pt}/nm) and alloy composition (at% Co) measured before and after aging in dry cell, PEMFC MEA and liquid electrolyte.

Sample/mode of TEM imaging	Nafion® 115 (MEA)/TEM	Nafion® 115 (dry cell)/IL-TEM	1 mol L^{-1} H_2SO_4/IL-TEM
d_{Pt} before	3.6 ± 1.2	3.8 ± 1.3	3.6 ± 1.2
d_{Pt} after	4.2 ± 1.5	3.8 ± 1.3	4.4 ± 1.2
at% Co before	19 ± 2	19 ± 2	25 ± 4
at% Co after	13 ± 2	18 ± 3	17 ± 4

For comparison, similar tests were performed with membrane electrode assemblies (MEA) baring a Pt_3Co/C cathode operated in unit-cell PEMFC at $T = 353$ K and fed with fully hydrated H_2/O_2 (1 atm/1 atm) or fully hydrated H_2/N_2 (1 atm/1 atm) during the acquisition of the polarization curves and AST, respectively. The MEA were of the catalyst-coated-backing (CCB) type, *i.e.* with the catalyst layers coated on the gas-diffusing layer. They were prepared using a Nafion® 115 membrane according to the filtration/brushing procedure described in [33] and featured 4.6 cm^2 of geometric electrode area. The catalyst layers were of Pt/C at the anode (0.4 mg_{Pt} cm^{-2}) and Pt_3Co/C at the cathode (0.4 mg_{Pt} cm^{-2}, which corresponds to *ca.* 0.43 mg_{Pt_3Co} cm^{-2}) and both comprised 35.5 wt% Nafion® ionomer. The experimental electrochemical surface area of the Pt_3Co/C cathode was 614 cm^2 (prior aging), *vs. ca.* 1670 cm^2 in theory (assuming the mass of Pt_3Co/C catalyst, its mean particle diameter and a $Pt_{0.81}Co_{0.19}$ alloy density of 19.6 g cm^{-3}, see Table 1), corresponding to an utilization factor of *ca.* 37%. CO-stripping voltammograms were also plotted by feeding the cell with fully hydrated H_2/CO and H_2/N_2 (1 atm/1 atm), the potential program and duration of the sequences under CO (resp. N_2) at the positive electrode being kept identical as in the dry cell or liquid electrolyte environment.

2.3. Identical location TEM (IL-TEM) procedures

In IL-TEM experiments, a suspension of 1 g L^{-1} of Pt_3Co/C, composed of 5 wt. % Nafion® solution (Aldrich) in 1:0.63 dry weight ratio, MQ-grade water and 20 wt.% Pt_3Co/C, was ultrasonically mixed for 30 min to obtain a well-dispersed ink. A 5 μL aliquot was then deposited over a gold TEM grid (300 mesh, Lacey Carbon; Agar Sc. UK), and dried in air. The TEM grid baring the catalytic ink composed of Pt_3Co/C powder and Nafion® was used as the working electrode in the dry cell and therefore kept in contact with the Nafion® 115 polymer electrolyte membrane during the AST and the electrochemical characterizations. The contact between the TEM grid and the Nafion® membrane was achieved by gently pressing the grid onto the Nafion® membrane with a graphite rod of the same diameter at the tip of which was attached a piece of carbon cloth; the rod was connected to the working electrode connection of the potentiostat using a gold wire.

The overall sequence of electrochemical characterizations/AST was kept identical whatever the nature of the working electrode (UMEC or TEM grid). The TEM images were used to qualitatively observe the changes of particles shape (change of sphericity, extent of agglomeration) and distribution over the carbon substrate, and to quantitatively follow the number and size of the nanoparticles

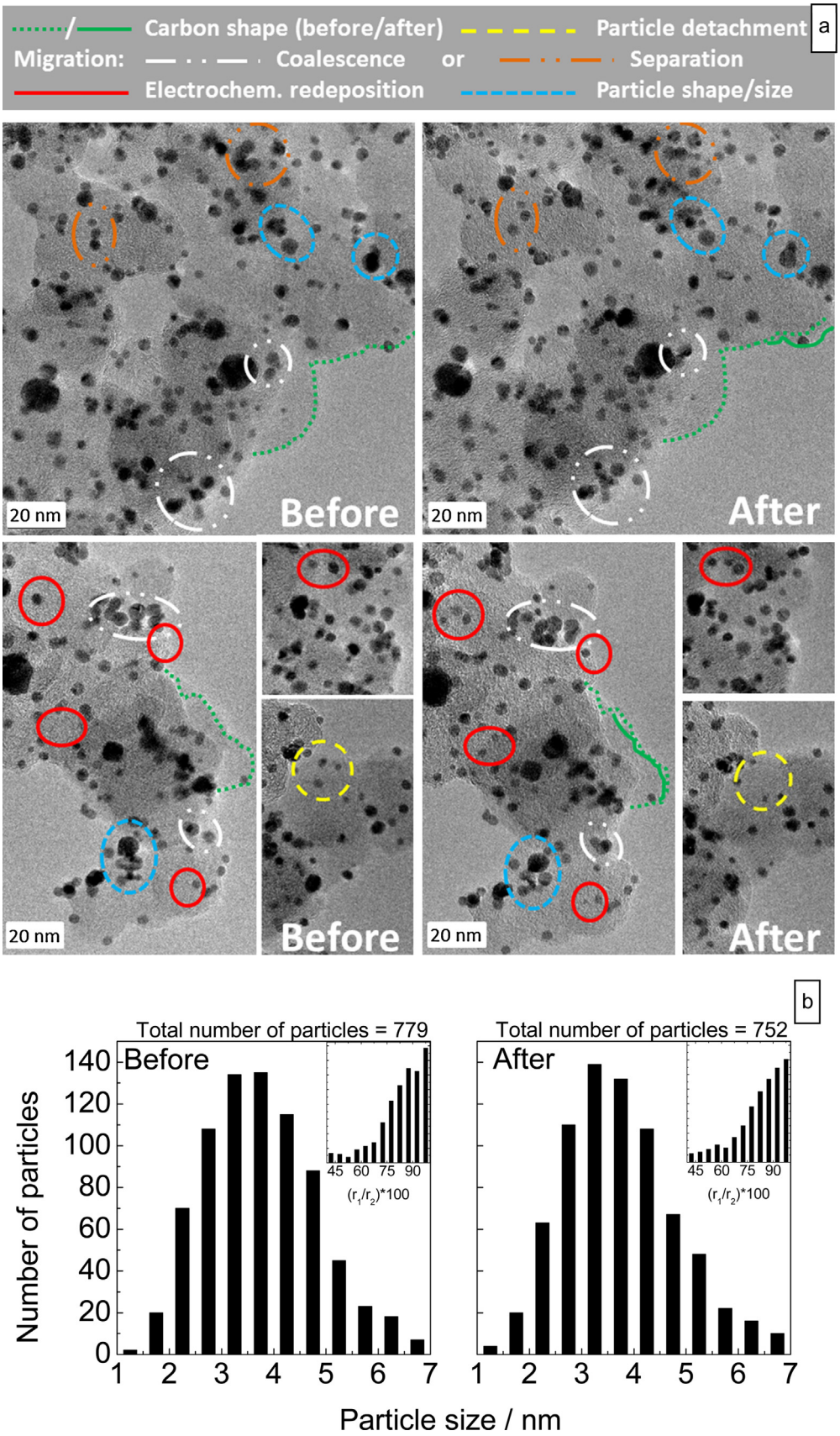

Fig. 1. (a) IL-TEM images of Pt_3Co/C nanoparticles before and after aging in dry cell (Nafion® 115 electrolyte) and (b) corresponding particle size distribution histograms. The (non-comprehensive) markers on the figure highlight representative examples of aging phenomena that occurred during the AST.

in similar regions of the Vulcan XC72 carbon prior/after the AST. To these goals, particle size distribution histograms were built following the methodology employed in [19]. Isolated and agglomerated nanoparticles were considered, the former ones exhibiting a simpler (*ca.* more circular) shape than the latter ones.

3. Results and discussion

Fig. 1 shows representative micrographs of the same Pt_3Co/C areas observed before and after aging in the dry cell. To the authors' knowledge, this is the first time that IL-TEM, developed in 2008 [31] for AST performed in liquid electrolyte [19,23–25,34–36], is used to probe the structural and chemical modifications of a Pt-M/C electrocatalyst in polymer electrolyte environment. For comparison, micrographs of the same Pt_3Co/C aged in single-cell PEMFC (TEM) and liquid electrolyte (IL-TEM) are presented in Supplementary Figs. S3 and S4, respectively.

The main aging phenomena that occurred during the AST in dry cell are (i) the migration of Pt_3Co/C nanocrystallites, either leading to agglomeration/coalescence (white dotted line) or separation (orange dotted line), (ii) their disappearance *via* dissolution or detachment (yellow dotted lines), (iii) their change of size/shape (blue dotted line) and (iv) the electrochemical redeposition of Pt^{z+} ions ($z = 2$ or 4, red line) *via* electrochemical Ostwald ripening, yielding new nanocrystallites. The color code in Fig. 1, Supplementary Fig. S4 and Ref. [19] is similar, which enables comparing the aging phenomena at stake during the AST in polymer *vs.* liquid electrolyte. On the one hand, some degradation mechanisms are observed whatever the nature of the electrolyte [23,31,37,38], *e.g.* migration of Pt_3Co/C nanocrystallites at the carbon surface and dissolution of the smallest Pt_3Co/C crystallites. In both cases, the number of nanoparticles present at the carbon substrate slightly decreases (Fig. 1, Supplementary Figs. S5 and 3-B in [19] for the results at the Nafion® and liquid interface, respectively). On the other hand, three differences are obvious: compared to liquid electrolyte, the polymer electrolyte induces (i) milder carbon corrosion, and in some regions (ii) significant Pt^{z+} redeposition (new particles are formed) and (iii) large particle Pt_3Co/C shape/size change. Whereas the histogram center slightly shifts to larger sizes, the particle sphericity is less depreciated (insets) after the aging in polymer than in liquid electrolyte, owing to smaller carbon corrosion in the former case (the migration/aggregation of Pt_3Co/C nanocrystallites is less facile). These differences may be rationalized by the smaller water content in the dry cell: water molecules activate the electrochemical corrosion of carbon [39,40] and of the metal nanocrystallites, but also enable "diluting" the Pt^{z+} ions (generated by the dissolution of small nanocrystallites) and favoring their diffusion away from the electrode (which limits their redeposition).

Thus, the electrochemical Ostwald ripening and the crystallite migration mechanisms prevail in polymer electrolyte *vs.* carbon corrosion [19] and crystallite detachment or irreversible dissolution [31,34,35] in liquid electrolyte. The influence of the polymer electrolyte is further demonstrated by the variation of the Pt:Co atomic composition. Whereas minor changes of the Co at% are monitored at the Pt_3Co/C | polymer electrolyte in the dry cell (Table 1), a large decrease of the Co at% is witnessed in liquid electrolyte. It is wise noting at that stage that the Co^{y+} ions formed by the corrosion of Pt_3Co/C nanoparticles cannot redeposit in PEMFC environment and remain trapped in the ionomer [29], where they are detected by X-EDS analyses; this does not correspond to metal Co atoms in the alloy and artificially heightens the Co at% measured after aging in dry cell. In addition, one would have noticed that upon PEMFC testing, the Co loss is somewhat similar to that in liquid electrolyte, and much larger than what witnessed in the dry cell; this can be rationalized by the fact that the PEMFC operates at higher

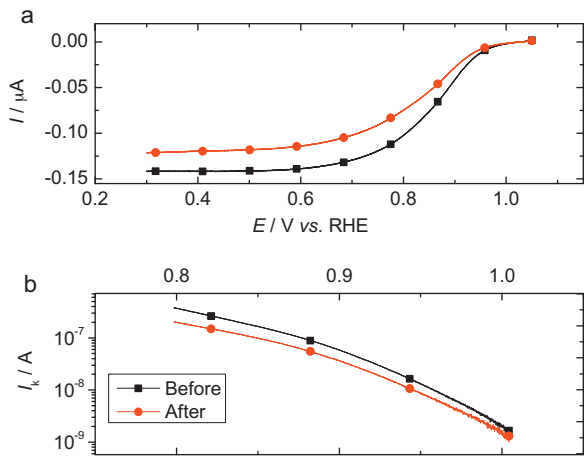

Fig. 2. (a) ORR voltamperograms plotted for Pt_3Co/C nanoparticles before and after aging in dry cell using a Nafion® 115 membrane as solid polymer electrolyte and (b) corresponding mass-transport-corrected Tafel plots.

temperature (80 °C) and under dynamic flux of fully hydrated gases, which favors a larger extent of washing of the Co^{y+} ions than in the dry cell, where the Pt_3Co/C catalyst is maintained in a cavity in which the only mass-transport process at stake is diffusion (at room temperature).

Similarly to what occurs in real PEMFC aging [41,42] or cation-contaminated perfluorosulfonated membranes [43], the poisoning of the sulfonic moieties of Nafion® by Co^{2+} ions lowers the diffusion rate of Co^{2+} ions from the outer Helmholtz plane, thereby slowing down Co dissolution from the alloy nanoparticles. On the contrary, the facile diffusion of Co^{2+} ions in the bulk of a liquid electrolyte provides a strong driving force to massive Co atoms dissolution. The IL-TEM micrographs also demonstrate that the intensity/nature of aging in Nafion® electrolyte depends on the region/location of the Pt_3Co/C nanoparticles observed, which was not obvious in liquid electrolyte [19]. In other words, the aging is more heterogeneous in solid electrolyte, as observed for PEMFC membrane-electrode assemblies (Supplementary Fig. S3 [42,44,45]), and confirmed by the broader particle-size distribution histograms after aging in polymer *vs.* liquid [19] electrolyte (Supplementary Figs. S4 and S5). Such heterogeneity originates from the incomplete electrocatalyst utilization (u_{Pt}) or effectiveness (ε_{Pt}) of volumic electrodes in interface with a polymer electrolyte [41,46]: in the MEA tested herein, u_{Pt} was worth *ca.* 37%, whereas it was slightly below 80% in the dry cell (*vs. ca.* 100% in liquid electrolyte, see Supplementary Fig. S2).

In summary, AST performed in liquid or polymer electrolyte induce different aging mechanisms and different extent of degradation. The morphological changes of the Pt_3Co/C nanoparticles are in average milder in polymer than in liquid electrolyte [19] and strongly depend on the region considered. The migration of the Pt-Co/C nanocrystallites and the redeposition of Pt^{z+} ions are favored *vs.* the electrochemical dissolution and carbon corrosion in liquid electrolyte.

Finally, the morphology and composition changes of the Pt_3Co/C nanoparticles were bridged to their electrocatalytic activity: overall, the aging resulted in reduced ORR activity in polymer electrolyte (Fig. 2 and Table 1), in opposition to the trend observed in liquid electrolyte [19]. The small nanoparticle size increase (positive effect on the intrinsic ORR activity) is negatively counter-balanced by Co-losses from the alloy [16,17,47] and by the trapping of the generated Co^{2+} ions in the ionomer phase at the vicinity of the remaining nanoparticles: both effects are detrimental to the oxygen mass-transport and electroreduction rates [29] (Table 2).

Table 2
Mass-transport and ohmic-drop corrected ORR specific activity (SA) of the Pt_3Co/C electrocatalyst measured before and after aging by potential stepping from 0.9 to 0.1 V *vs.* RHE in dry cell, PEMFC MEA and liquid electrolyte.

Electrolyte	Sample	SA @ 0.85 V μA cm^{-2}_{Pt}		SA @ 0.90 V μA cm^{-2}_{Pt}	
		Before	After	Before	After
Nafion® 115 (dry cell)	Pt_3Co/C	56	32	17	11
Nafion® 115 (MEA)	Pt_3Co/C [$]	265	217	18	21
	Pt_3Co/C [#]	50	41	3.4	3.9
1 mol L^{-1} H_2SO_4	Pt_3Co/C [*]	84	83	20	20

[$], [#] and [*] are values measured at 353 K, recalculated at 298 K using an activation energy of 24 kJ mol^{-1} [48,49] and reproduced from Ref. [19], respectively.

4. Conclusion

For the first time, state-of-the-art nanostructured Pt_3Co/C electrocatalysts were submitted to accelerated stress tests in dry electrochemical environment (using a Nafion® 115 membrane as polymer electrolyte) and characterized in terms of electrocatalytic activity (using an ultramicroelectrode with cavity) and in terms of structure and composition by Identical Location Transmission Electron Microscopy prior/after these AST, in conditions that perfectly mimic real PEMFC operation. Thanks to the unique setup used herein, it was possible to bridge the structure and composition changes of the Pt_3Co/C nanoparticles to their electrocatalytic activity prior/after the AST without interference with any characterization in liquid electrolyte medium. Furthermore, by comparison with anterior results from the literature (some of which in our group), this also enabled to compare the fate of such state-of-the-art electrocatalyst material upon aging in Nafion® environment with that in conventional liquid electrolyte, in which AST are usually performed. The present results demonstrate that the Pt_3Co/C nanoparticles are modified upon aging at Nafion® interface, in agreement with results from similar tests in unit PEFMC; however, the main degradation processes differ to those monitored in liquid electrolyte (smaller carbon corrosion but larger Pt redeposition processes are witnessed in the former case) and are overall milder in magnitude. Nevertheless, these milder material degradations result in larger decrease of the ORR intrinsic activity of the Pt_3Co/C nanoparticles. These peculiar findings result from the absence of liquid water and the lack of ion mobility within the Nafion® membrane. Furthermore, this study shows that although interesting from a fundamental viewpoint, AST performed in liquid electrolyte environment do not relevantly mimic the fate of Pt_3Co/C electrocatalysts in PEMFC environment and can therefore not be directly used to predict how the nanostructured electrocatalyst will behave in long-term PEMFC testing.

Acknowledgments

The authors thank CAPES-COFECUB (Project Ph 598/08) and Oseo H2E for funding. We thank the UMEC French CNRS network for providing the UMEC, as well as Vincent Vivier and Axel Desnoyers de Marbaix for their participation in the design and realization of the dry cell. MC thanks the French University Institute (IUF) for its support.

Appendix A. Supplementary data

Supplementary material related to this article can be found, in the online version, at http://dx.doi.org/10.1016/j.apcatb.2014.03.029.

References

[1] H.A. Gasteiger, W. Vielstich, H. Yokokawa, Handbook of Fuel Cells, John Wiley & Sons Ltd., Chichester, 2009.
[2] W. Vielstich, A. Lamm, H.A. Gasteiger, Handbook of Fuel Cells, Wiley, Chichester, 2003.
[3] H.A. Gasteiger, S.S. Kocha, B. Sompalli, F.T. Wagner, Appl. Catal. B: Environ. 56 (2005) 9–35.
[4] S. Koh, P. Strasser, J. Electrochem. Soc. 157 (2010) B585–B591.
[5] K.C. Neyerlin, R. Srivastava, C.F. Yu, P. Strasser, J. Power Sources 186 (2009) 261–267.
[6] J. Greeley, StephensF I.E.L., A.S. Bondarenko, T.P. Johansson, H.A. Hansen, T.F. Jaramillo, J. Rossmeisl, I. Chorkendorff, J.K. Nørskov, Nat. Chem. 1 (2009) 552–556.
[7] V.R. Stamenkovic, B. Fowler, B.S. Mun, G.F. Wang, P.N. Ross, C.A. Lucas, N.M. Markovic, Science 315 (2007) 493–497.
[8] O. Antoine, Y. Bultel, R. Durand, P. Ozil, Electrochim. Acta 43 (1998) 3681–3691.
[9] K. Kinoshita, J. Electrochem. Soc. 137 (1990) 845–848.
[10] Y. Takasu, N. Ohashi, X.G. Zhang, Y. Murakami, H. Minagawa, S. Sato, K. Yahikozawa, Electrochim. Acta 41 (1996) 2595–2600.
[11] V.R. Stamenkovic, B.S. Mun, M. Arenz, K.J.J. Mayrhofer, C.A. Lucas, G.F. Wang, P.N. Ross, N.M. Markovic, Nat. Mater. 6 (2007) 241–247.
[12] F.J. Perez-Alonso, D.N. McCarthy, A. Nierhoff, P. Hernandez-Fernandez, C. Strebel, I.E.L. Stephens, J.H. Nielsen, I. Chorkendorff, Angew. Chem. Int. Ed. 51 (2012) 4641–4643.
[13] M. Chatenet, E. Guilminot, C. Iojoiu, J.-Y. Sanchez, E. Rossinot, F. Maillard, ECS Trans. 11 (2007) 1203–1214.
[14] L. Dubau, J. Durst, F. Maillard, M. Chatenet, J. Andre, E. Rossinot, ECS Trans. 33 (2010) 399–405.
[15] L. Dubau, F. Maillard, M. Chatenet, J. Andre, E. Rossinot, ECS Trans. 33 (2010) 407–417.
[16] L. Dubau, F. Maillard, M. Chatenet, L. Guetaz, J. Andre, E. Rossinot, J. Electrochem. Soc. 157 (2010) B1887–B1895.
[17] F. Maillard, L. Dubau, J. Durst, M. Chatenet, J. André, E. Rossinot, Electrochem. Commun. 12 (2010) 1161–1164.
[18] C. Cui, L. Gan, M. Heggen, S. Rudi, P. Strasser, Nat. Mater. 12 (2013) 765–771.
[19] F. Nikkuni, E. Ticianelli, L. Dubau, M. Chatenet, Electrocatalysis 4 (2013) 104–116.
[20] H.R. Colon-Mercado, H. Kim, B.N. Popov, Electrochem. Commun. 6 (2004) 795–799.
[21] H.R. Colon-Mercado, B.N. Popov, J. Power Sources 155 (2006) 253–263.
[22] S.C. Zignani, E. Antolini, E.R. Gonzalez, J. Power Sources 182 (2008) 83–90.
[23] K. Schlogl, M. Hanzlik, M. Arenz, J. Electrochem. Soc. 159 (2012) B677–B682.
[24] K. Hartl, M. Hanzlik, M. Arenz, Energy Environ. Sci. 4 (2011) 234–238.
[25] K.J.J. Mayrhofer, S.J. Ashton, J.C. Meier, G.K.H. Wiberg, M. Hanzlik, M. Arenz, J. Power Sources 185 (2008) 734–739.
[26] Z. Siroma, M. Tanaka, K. Yasuda, K. Tanimoto, M. Inaba, A. Tasaka, Electrochemistry 75 (2007) 258–260.
[27] N. Takeuchi, T.F. Fuller, in: T. Fuller, K. Shinohara, V. Ramani, P. Shirvanian, H. Uchida, S. Cleghorn, M. Inaba, S. Mitsushima, P. Strasser, H. Nakagawa, H.A. Gasteiger, T. Zawodzinski, C. Lamy (Eds.), Proton Exchange Membrane Fuel Cells 8, Pts 1 and 2, Electrochemical Society Inc., Pennington, 2008, pp. 1563–1571.
[28] J. Xie, D.L. Wood, D.M. Wayne, T.A. Zawodzinski, P. Atanassov, R.L. Borup, J. Electrochem. Soc. 152 (2005) A104–A113.
[29] J. Durst, M. Chatenet, F. Maillard, Phys. Chem. Chem. Phys. 14 (2012) 13000–13009.
[30] B. Vion-Dury, M. Chatenet, V. Vivier, 220th ECS Meeting of the Electrochemical Society, The Electrochemical Society, Boston, 2011.
[31] K.J.J. Mayrhofer, J.C. Meier, S.J. Ashton, G.K.H. Wiberg, F. Kraus, M. Hanzlik, M. Arenz, Electrochem. Commun. 10 (2008) 1144–1147.
[32] E. Guilminot, A. Corcella, M. Chatenet, F. Maillard, J. Electroanal. Chem. 599 (2007) 111–120.
[33] V.A. Paganin, E.A. Ticianelli, E.R. Gonzalez, J. Appl. Electrochem. 26 (1996) 297–304.
[34] A. Zana, J. Speder, M. Roefzaad, L. Altmann, M. Baumer, M. Arenz, J. Electrochem. Soc. 160 (2013) F608–F615.
[35] F.J. Perez-Alonso, C.F. Elkjær, S.S. Shim, B.L. Abrams, I.E.L. Stephens, I. Chorkendorff, J. Power Sources 196 (2011) 6085–6091.
[36] L. Dubau, L. Castanheira, G. Berthomé, F. Maillard, Electrochim. Acta 110 (2013) 273–281.
[37] Y. Yu, H.L. Xin, R. Hovden, D. Wang, E.D. Rus, J.A. Mundy, D.A. Muller, H.D. Abruña, Nano Lett. 12 (2012) 4417–4423.
[38] K. Hartl, M. Nesselberger, K.J.J. Mayrhofer, S. Kunz, F.F. Schweinberger, G. Kwon, M. Hanzlik, U. Heiz, M. Arenz, Electrochim. Acta 56 (2010) 810–816.
[39] J.P. Meyers, R.M. Darling, J. Electrochem. Soc. 153 (2006) A1432–A1439.

[40] N. Takeuchi, T.F. Fuller, J. Electrochem. Soc. 157 (2010) B135–B140.
[41] L. Dubau, M. Lopez-Haro, L. Castanheira, J. Durst, M. Chatenet, P. Bayle-Guillemaud, L. Guétaz, N. Caqué, E. Rossinot, F. Maillard, Appl. Catal. B: Environ. 142–143 (2013) 801–808.
[42] J. Durst, A. Lamibrac, F. Charlot, J. Dillet, L.F. Castanheira, G. Maranzana, L. Dubau, F. Maillard, M. Chatenet, O. Lottin, Appl. Catal. B: Environ. 138–139 (2013) 416–426.
[43] B. Kienitz, B. Pivovar, T. Zawodzinski, F.H. Garzon, J. Electrochem. Soc. 158 (2011) B1175–B1183.
[44] A. Lamibrac, G. Maranzana, J. Dillet, O. Lottin, S. Didierjean, J. Durst, L. Dubau, F. Maillard, M. Chatenet, Energy Procedia 29 (2012) 318–324.
[45] L. Dubau, J. Durst, F. Maillard, M. Chatenet, L. Guétaz, J. André, E. Rossinot, Fuel Cells 12 (2012) 188–198.
[46] M. Chatenet, L. Dubau, N. Job, F. Maillard, Catal. Today 156 (2010) 76–86.
[47] L. Dubau, F. Maillard, M. Chatenet, J. André, E. Rossinot, Electrochim. Acta 56 (2010) 776–783.
[48] A. Velázquez-Palenzuela, F. Centellas, E. Brillas, C. Arias, R.M. Rodríguez, J.A. Garrido, P.-L. Cabot, Int. J. Hydrogen Energy 37 (2012) 17828–17836.
[49] V. Stamenković, T.J. Schmidt, P.N. Ross, N.M. Marković, J. Electroanal. Chem. 554-555 (2003) 191–199.